Available online at www.CivileJournal.org

Civil Engineering Journal

(E-ISSN: 2476-3055; ISSN: 2676-6957)

Vol. 12, No. 10, October, 2026



Incremental Dynamic Analysis of Seismic Fragility in RC Columns with Varying Reinforcement Ratios

Joe Robert Paul G. Lucena [1, 2*], Franklyn F. Manggapis [3], Luigi Carlo M. De Jesus [1, 2], Alibek Adilbekov [2, 4], Shakhnoza Makhmudova [2, 5], Kamola Mannapova [2, 5]

[1] *School of Engineering, Asia Pacific College, Makati City 1232, Philippines.*

[2] *Naveen Jindal Young Global Research Fellowship, O.P. Jindal Global University, Haryana 131001, India.*

[3] *Civil Engineering Department, Far Eastern University Alabang, Muntinlupa City 1781, Philippines.*

[4] *M. Kozybayev North Kazakhstan University, Petropavlovsk 150000, Kazakhstan.*

[5] *Tashkent State Transport University, Tashkent 100123, Uzbekistan.*

Received 16 June 2026; Revised 07 September 2026; Accepted 24 September 2026; Published 01 October 2026

Abstract

This study evaluates the influence of longitudinal reinforcement ratios on the model-predicted seismic fragility of reinforced-concrete (RC) cantilever columns. By holding geometry, materials, loading, and modeling formulation constant, four 300 × 300 mm, 4.0 m-high numerical columns with varying reinforcement ratios (6.55%, 4.19%, 2.79%, and 2.18%) were analyzed in SeismoStruct to isolate the comparative influence of steel content on drift-based fragility. Seven horizontal records from the 1989 Mw 6.9 Loma Prieta earthquake were incrementally scaled using peak ground acceleration (PGA) as the intensity measure. Maximum drift ratio served as the engineering demand parameter, with lognormal fragility functions fitted for 0.5%, 0.7%, 1.5%, 2.5%, and 5.0% drift thresholds. Results demonstrate that the mean PGA required to reach a 5.0% drift decreased from 1.85g for the most heavily reinforced column to 1.42g, 1.07g, and 0.95g as reinforcement decreased. While performance differences between the columns were small or non-monotonic at lower thresholds, they became clear at severe drift levels, accompanied by increased record-to-record dispersion for the least reinforced model. Ultimately, this controlled comparison highlights that reinforcement effects depend significantly on the selected drift severity and fitted dispersion, providing simulation-based, relative threshold-exceedance trends rather than evidence of experimentally validated physical collapse.

Keywords: Incremental Dynamic Analysis; Fragility Curves; Seismic Vulnerability; Dynamic Analysis; Seismic Analysis.

1. Introduction

Performance-based earthquake engineering requires probabilistic measures because structural response varies with both shaking intensity and record characteristics. Incremental Dynamic Analysis (IDA) addresses this need by subjecting a nonlinear structural model to multiple ground-motion records that are progressively scaled until specified response thresholds are reached [1]. The resulting intensity-measure–demand relationships can be converted into fragility curves that express the conditional probability of exceeding a defined limit state. Earlier applications established the value of nonlinear dynamic analysis and fragility methods for probabilistic seismic assessment [2-5], while also showing that the repeated analyses required by IDA can impose a substantial computational burden [6-8].

* Corresponding author: joerobertpaull@apc.edu.ph

https://doi.org/10.28991/CEJ-2026-012-010-04

© 2026 by the authors. Licensee C.E.J, Tehran, Iran. This article is an open access article distributed under the terms and conditions of the Creative Commons Attribution (CC-BY) license (http://creativecommons.org/licenses/by/4.0/).

For reinforced-concrete (RC) columns, lateral response is governed by interacting parameters that include longitudinal-reinforcement ratio, reinforcement grade, axial-load level, transverse confinement, shear-span ratio, and material constitutive behavior. Trejo et al. [9] showed that reinforcement grade and ratio affect column resistance, ductility, and energy dissipation. Studies of high-performance and steel-reinforced concrete columns similarly indicate that the effect of longitudinal steel depends on axial loading, confinement, and the governing failure mechanism [10–12]. Refined deformation limits for RC bridge columns further demonstrate that the selected damage criterion can materially influence performance classification [13]. Therefore, increasing the reinforcement ratio should not be assumed to produce a proportional reduction in vulnerability at every response level.

Recent studies published in 2025–2026 have clarified both the capabilities and limitations of numerical column assessment. Di Domenico et al. [14] calibrated fiber-based models of flexure-controlled RC columns against tests and emphasized the influence of cover and core concrete, strain penetration, and bar buckling or fracture. Zhang et al. [15] demonstrated that drift alone may not consistently represent experimentally observed damage under bidirectional loading. Recent fragility studies of RC bridge piers examined retrofit effects, deterioration, and record-to-record uncertainty [16, 17]. In parallel, combined experimental and numerical investigations highlighted the need to reproduce stiffness, strength, cyclic deterioration, bond-slip behavior, and flexure–shear failure modes when validating analytical models [18, 19]. Collectively, these works show that fragility estimates depend on the constitutive model, ground-motion set, intensity measure, and limit-state definition.

Despite these advances, the literature provides limited controlled evidence on how longitudinal-reinforcement ratio alone shifts a complete family of drift-based fragility curves for otherwise comparable RC cantilever columns. Many studies investigate full structural systems, strengthened or deteriorated members, or configurations in which several design variables change simultaneously [5, 16, 17, 20]. This makes it difficult to isolate reinforcement-ratio effects across several response thresholds. A further interpretive gap concerns the use of "collapse" for a numerically exceeded drift limit when dynamic instability, loss of axial-load capacity, or local failure mechanisms have not been demonstrated [21, 22].

This study addresses the identified gap through a controlled numerical comparison of four 300 × 300 mm, 4.0 m RC cantilever-column models with longitudinal-reinforcement ratios of 6.55%, 4.19%, 2.79%, and 2.18%. Geometry, material properties, boundary conditions, the 20 kN applied axial load, and ground-motion inputs were held constant while the longitudinal reinforcement was varied. Seven records from the 1989 Loma Prieta earthquake were incrementally scaled in SeismoStruct, using peak ground acceleration (PGA) as the intensity measure and maximum drift ratio as the engineering demand parameter. PGA thresholds corresponding to drift ratios of 0.50%, 0.70%, 1.50%, 2.50%, and 5.00% were fitted with lognormal distributions. The workflow is summarized in Figure 1. The study quantifies threshold shifts and record-to-record dispersion while treating the 5.00% state as an analytical drift proxy, not demonstrated physical collapse. Its scope is limited to numerical simulation and does not constitute experimental validation.

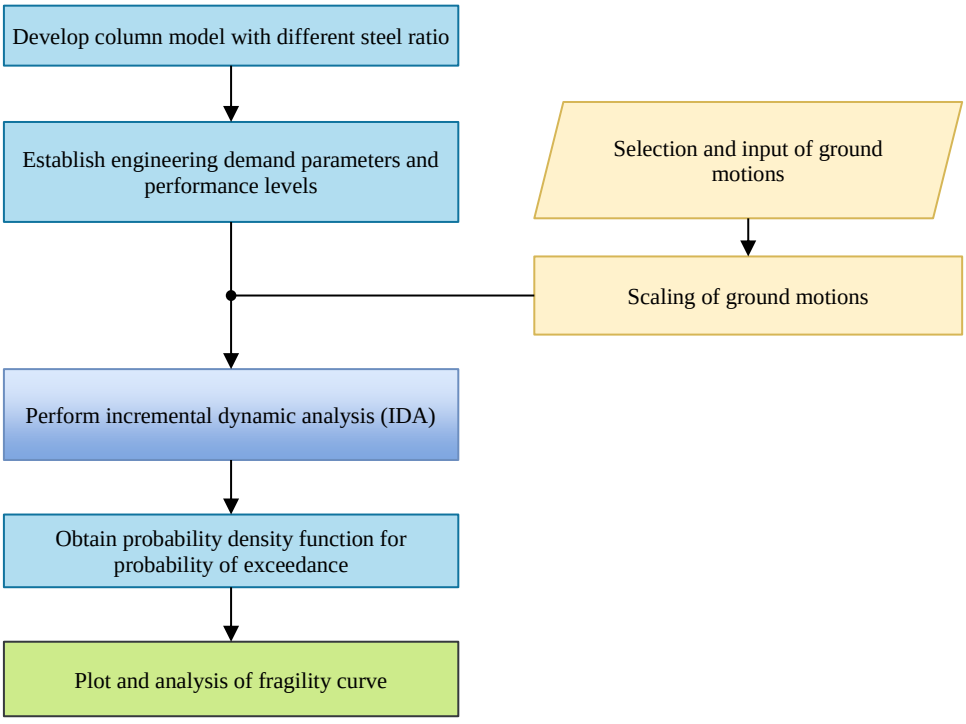
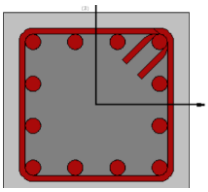
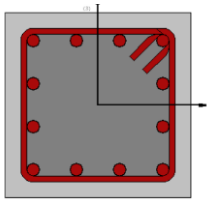
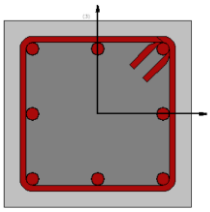
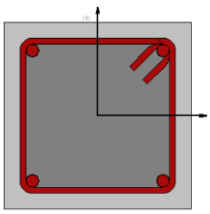


Figure 1. Flowchart of the research methodology

2. Methodology

The study follows the flowchart presented in Figure 1. The analysis begins with the modeling of the reinforced concrete columns. Four columns were considered, each with a different steel ratio due to varying amounts of longitudinal reinforcement (see Table 1). However, all columns have the same geometry (cross-sectional dimensions and height). The concrete follows the nonlinear concrete model of Mander et al. [23], while the steel follows the Menegotto–Pinto steel model [24].

Table 1. Details of reinforced concrete columns

Column	Longitudinal Reinf.	Steel Ratio	Cross-Section	First-Mode Period
C1	12 – 25 mm dia.	6.55%		0.3258 s
C2	12 – 20 mm dia.	4.19%		0.3325 s
C3	8 – 20 mm dia.	2.79%		0.3373 s
C4	4 – 25 mm dia.	2.18%		0.3417 s

Column dimension: 300 mm × 300 mm; Column height = 4,000 mm; Compressive strength = 28 MPa; Yield strength of longitudinal reinforcement = 420 MPa; Yield strength of transverse reinforcement = 275 MPa

2.1. Performance Levels and Engineering Demand Parameters

There are several ways to evaluate the performance level of columns. Some examples include damage due to material strain [13, 25], curvature ductility [13], displacement [26], and energy dissipation [20], among others. In this paper, the engineering demand parameter used to evaluate the structure is based on drift ratio. This is because the column stands vertically and is fixed at the base, where the ground acceleration is applied. The corresponding limit states for this study follow the related fragility framework of Kim and Shinozuka [27], with the drift-based damage-state thresholds adopted from Dutta and Mander [28], as presented in Table 2. These limit states are also used in analyzing the performance level of columns in bridges.

Table 2. Limit states and performance levels

Limit State	Description	Performance Level
LS1	Almost No Damage	0.50%
LS2	Slight Damage	0.70%
LS3	Moderate Damage	1.50%
LS4	Extensive Damage	2.50%
LS5	Collapse	5.00%

2.2. Selection of Ground Motion Records and Identification of Materials

Ground motion records were obtained from the PEER NGA-West2 database. The web-based Pacific Earthquake Engineering Research Center (PEER) ground motion database provides tools for searching, selecting, and downloading ground motion data [29]. For this analysis, ground motion records from the Mw 6.9 Loma Prieta earthquake were selected. The number of required ground motion records varies according to different standards. ASCE 7-05 / ASCE 7-10 requires 3 ground motion records, while the newer ASCE 7-16 requires 11 ground motion records for probabilistic seismic assessment. In the Philippines, DPWH BSDS 2013 requires seven ground motion records for a probabilistic site-specific seismic hazard assessment. In this study, seven ground motion records from the Loma Prieta earthquake are used.

The ground motion records were scaled to undertake IDA. IDA subjects a structural model to a suite of real ground motion records, each scaled to increasing levels of intensity [2-4]. Scaling ground motions strategically, with increments designed to capture performance close to the desired limit states, is essential for performing statistical assessment of performance limits. Software such as SeismoMatch is capable of scaling ground motion records from various databases. However, SeismoStruct has an Incremental Dynamic Analysis option where ground motions are scaled directly within the structural analysis. In this study, scaling ground motions first involved identifying the scale at which the structure reached the highest limit state. Then, the scale interval was set so that the remaining limit states could be reached exactly or closely approximated. Large intervals or deviations from the target limit state reduce the accuracy of the results. This method follows the strategy of the Hunt-and-Fill method proposed by Vamvatsikos and Cornell [1].

To accurately capture the nonlinear behavior of the columns under dynamic loading, detailed material constitutive models were defined for the analysis. The concrete was modeled using the Mander et al. nonlinear concrete model [23]. The specific parameters defined for the concrete included an unconfined compressive strength of 28 MPa, a tensile strength of 2.2 MPa, a modulus of elasticity of 24.87 GPa, a strain at peak stress of 0.002 m/m, and a specific weight of 24.00 kN/m³. The reinforcing steel was governed by the Menegotto–Pinto steel model. For both the longitudinal and transverse reinforcement, the steel was assigned a modulus of elasticity of 200 GPa, a fracture/buckling strain of 0.20, and a specific weight of 78.00 kN/m³. To accurately represent the cyclic behavior and the Bauschinger effect, the steel model incorporated a strain hardening parameter of 0.005, an initial shape parameter of 20.00 for the transition curve, transition curve shape calibrating coefficients A1 and A2 of 18.50 and 0.15, respectively, and isotropic hardening calibrating coefficients A3 and A4 of 0.00 and 1.00, respectively. The yield strength was set to 420 MPa for the longitudinal reinforcement and 275 MPa for the transverse reinforcement [24].

2.3. Incremental Dynamic Analysis

In this study, IDA was performed using SeismoStruct. First, the material properties for the concrete column, including those of concrete and steel, were defined. Subsequently, the cross-sections were defined, along with the configuration of longitudinal and transverse reinforcement. Four columns with different steel ratios, as listed in Table 1, were modeled. These columns were represented as inelastic plastic-hinge force-based frame elements. The ground motions downloaded from the PEER NGA-West2 database, particularly their acceleration-time histories, were then uploaded to SeismoStruct.

The column base is fully restrained in all degrees of freedom, while the top is free to displace and rotate. Each column is subjected to a 20 kN downward concentrated force at the top. For the dynamic analysis, this 20 kN load was converted to an equivalent lumped seismic mass (approx. 2.04 t) at the free end of the column to accurately capture inertial effects. The acceleration-time history is applied as an acceleration load at the base, as shown in Figure 2. Using the incremental dynamic analysis option, the drift of the column's top end relative to its base is then determined for every scale of each ground motion.

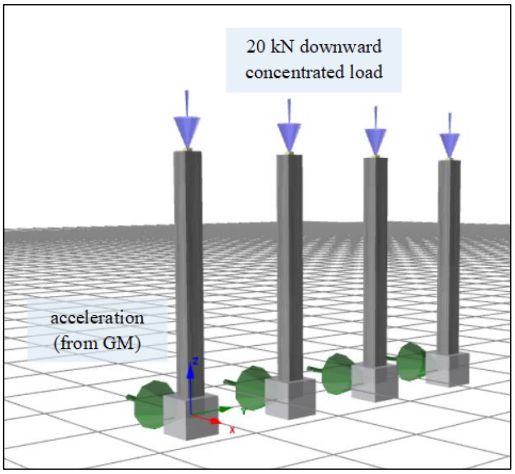


Figure 2. Reinforced concrete columns with applied loads

2.4. Statistical Analysis and Development of the Probability Density Function for the Probability of Exceedance

Drift ratios are obtained for each performance level. As a result, each ground motion yields a PGA value for every limit state, resulting in seven samples per limit state. These PGA values, for each ground motion at every limit state, are determined using linear interpolation or spline polynomial interpolation.

For each limit state, a statistical analysis is performed where the seven PGA values are used to determine the probability density function. The mean, μ, and standard deviation, σ, of the PGA values from the different ground motions are then calculated for each limit state. The lognormal values of these measures are subsequently obtained using the lognormal transformation equations of Nowak and Collins, as presented in Equations 1 and 2 [30], where ${\sigma^2}_{\ln(X)}$ is the variance of the lognormal distribution of the variable X and V_X is the coefficient of variation of X.

$$ {\sigma^2}_{\ln(X)} = \ln({V^2}_X + 1) \quad (1) $$

$$ \mu_{\ln(X)} = \ln(\mu) - \frac{1}{2}{\sigma^2}_{\ln(X)} \quad (2) $$

From the lognormal mean and standard deviation values, the probability of a drift ratio being equal to or greater than a given Limit State (LS), also known as the probability of exceedance, is defined in Equation 3, where $P_f(\geq R)$ is the probability of exceedance (failure probability) and Φ is the standard normal cumulative distribution function (CDF).

$$ P_f(\geq R) = \Phi\left[\frac{\ln X - \mu_{\ln(X)}}{\sigma_{\ln(X)}}\right] \quad (3) $$

PGA values are then substituted into this equation at regular intervals until a 100% probability of exceedance is reached. This indicates a 100% chance that this PGA will cause a drift ratio equal to or greater than the limit state being analyzed. Finally, the fragility curves for the columns, considering the five limit states, are plotted. These fragility curves are essential tools for seismic risk assessments, enabling engineers and decision-makers to evaluate the likelihood of structural failure and develop effective mitigation strategies.

3. Results and Discussion

3.1. Selected Ground Motion Records

Table 3 identifies the seven PEER NGA-West2 records used in the analyses. All were recorded during the 1989 Mw 6.9 Loma Prieta earthquake [29, 31]. The suite therefore supports a controlled comparison among C1–C4 but represents only within-event variability.

Table 3. Ground motion records from Loma Prieta earthquake

RSN (Record Sequence Number)	Earthquake event	Year	Location Recorded
731	Loma Prieta	1989	APEEL 10 - Skyline
736	Loma Prieta	1989	APEEL 9 - Crystal Springs Res
742	Loma Prieta	1989	Bear Valley #1, Fire Station
748	Loma Prieta	1989	Belmont - Envirotech
754	Loma Prieta	1989	Coyote Lake Dam (Downst)
760	Loma Prieta	1989	Foster City - Menhaden Court
762	Loma Prieta	1989	Fremont - Mission San Jose

The original PGA values obtained using SeismoMatch 2025 are listed in Table 4. In the table, g denotes standard gravitational acceleration (9.80665 m/s²), and RSN denotes the PEER record sequence number.

Table 4. PGA of different ground motions

RSN	PGA (m/s²)	PGA (g)
731	0.37	0.04
736	0.48	0.05
742	0.71	0.07
748	1.09	0.11
754	1.57	0.16
760	1.08	0.11
762	1.24	0.13

The ground motions listed in Tables 3 and 4 were uploaded to SeismoStruct. Using the IDA option, these ground motions were scaled by various factors. These scaling factors were chosen based on the intended limit states; specifically, they were determined so that the drift ratio reached at least 5.0%.

The maximum drift ratio, as defined in Equation 4, was determined for each ground motion at every applied scale factor. These drift ratios were then compared to the corresponding PGA for each scaling factor. The data points for drift ratio and PGA are presented in Figure 3. It is evident that data points at lower PGA values show less dispersion compared to those at higher PGA values. Additionally, Column 1 (C1), which has the highest stiffness among the columns, exhibits a more uniform, tighter distribution of data points at the same PGA values than the other columns. Conversely, data points are more dispersed at higher PGA values and for columns with greater flexibility.

$$Drift\ Ratio\ (\%) = \frac{Drift}{Height\ of\ col.} \times 100 \tag{4}$$

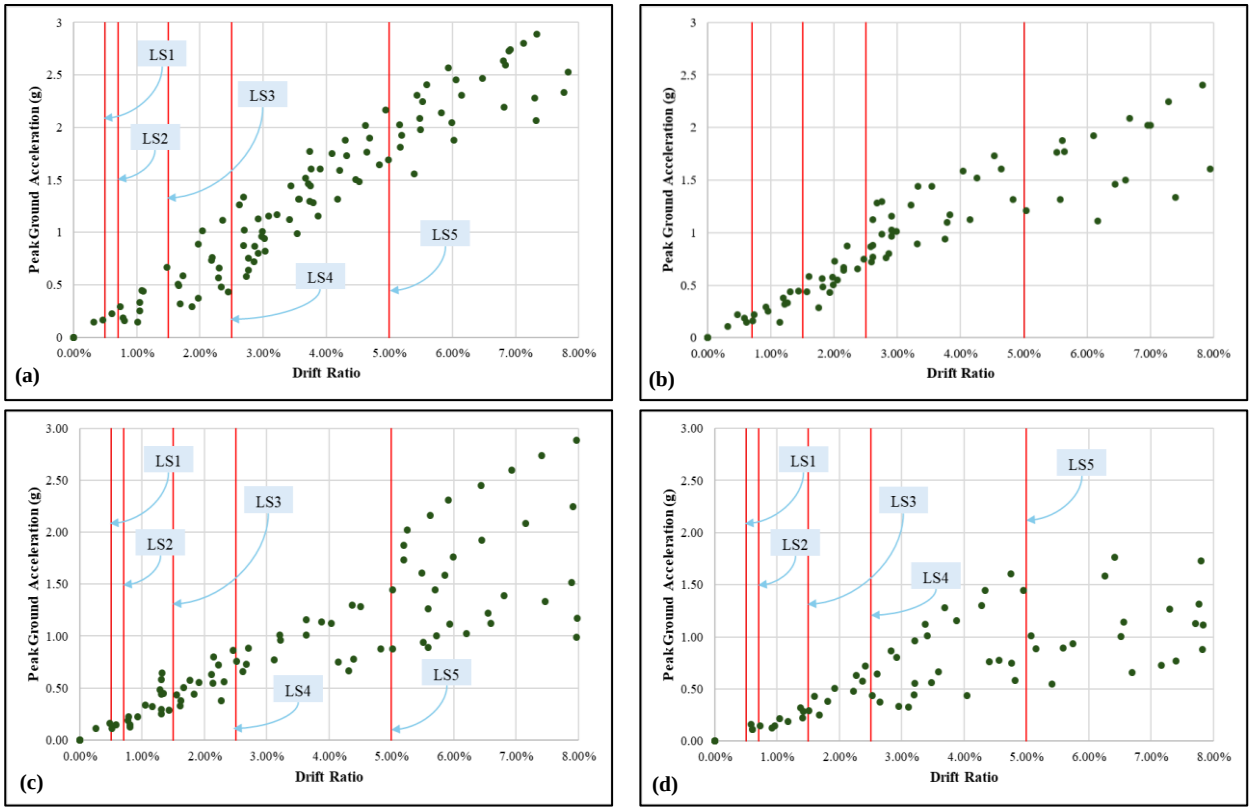


Figure 3. IDA relationships between maximum drift ratio and scaled PGA for (a) C1, (b) C2, (c) C3, and (d) C4

As previously discussed, the PGA values for each ground motion at every limit state were determined using either linear interpolation or spline polynomial interpolation. These values are presented in Tables 5 to 8.

Table 5. PGA threshold statistics and fitted lognormal parameters for C1

RSN	PGA at Limit States (in g)				
	0.50%	**0.70%**	**1.50%**	**2.50%**	**5.00%**
731	0.12	0.17	0.30	0.64	1.69
736	0.23	0.28	0.53	0.82	1.93
742	0.07	0.10	0.23	0.46	2.18
748	0.18	0.27	0.68	1.21	1.53
754	0.10	0.14	0.29	0.54	1.87
760	0.18	0.23	0.45	0.70	1.73
762	0.12	0.17	0.44	1.21	2.00
Mean	0.14	0.19	0.42	0.80	1.85
Standard Dev.	0.05	0.06	0.15	0.28	0.20
Squared COV	0.13	0.10	0.12	0.12	0.01
Lognormal values:					
Variance	0.12	0.10	0.12	0.12	0.01
Mean	-2.01	-1.69	-0.93	-0.28	0.61
Log Std. Dev.	0.35	0.31	0.34	0.34	0.11

Table 6. PGA threshold statistics and fitted lognormal parameters for C2

RSN	PGA at Limit States (in g)				
	0.50%	**0.70%**	**1.50%**	**2.50%**	**5.00%**
731	0.16	0.23	0.47	0.75	1.24
736	0.12	0.19	0.54	0.94	1.33
742	0.06	0.09	0.23	0.70	1.79
748	0.23	0.27	0.46	0.73	1.02
754	0.11	0.16	0.40	0.72	1.67
760	0.16	0.21	0.42	0.72	1.20
762	0.13	0.19	0.39	0.66	1.65
Mean	0.14	0.19	0.41	0.75	1.42
Standard Dev.	0.05	0.05	0.09	0.08	0.27
Squared COV	0.12	0.08	0.05	0.01	0.04
Lognormal values:					
Variance	0.11	0.08	0.05	0.01	0.04
Mean	-2.02	-1.70	-0.91	-0.30	0.33
Log Std. Dev.	0.33	0.28	0.21	0.11	0.19

Table 7. PGA threshold statistics and fitted lognormal parameters for C3

RSN	PGA at Limit States (in g)				
	0.50%	**0.70%**	**1.50%**	**2.50%**	**5.00%**
731	0.12	0.17	0.28	0.58	0.87
736	0.13	0.17	0.60	0.71	0.89
742	0.09	0.12	0.37	0.87	1.37
748	0.16	0.20	0.48	0.58	0.84
754	0.16	0.21	0.68	0.86	1.44
760	0.11	0.16	0.31	0.63	0.88
762	0.08	0.11	0.33	0.75	1.22
Mean	0.12	0.16	0.44	0.71	1.07
Standard Dev.	0.03	0.03	0.14	0.11	0.24
Squared COV	0.06	0.04	0.11	0.02	0.05
Lognormal values:					
Variance	0.06	0.04	0.10	0.02	0.05
Mean	-2.14	-1.83	-0.88	-0.35	0.04
Log Std. Dev.	0.25	0.21	0.32	0.16	0.22

Table 8. PGA threshold statistics and fitted lognormal parameters for C4

RSN	PGA at Limit States (in g)				
	0.50%	**0.70%**	**1.50%**	**2.50%**	**5.00%**
731	0.08	0.11	0.23	0.36	0.80
736	0.10	0.14	0.29	0.44	0.60
742	0.08	0.11	0.36	0.75	1.45
748	0.09	0.13	0.23	0.30	0.83
754	0.14	0.18	0.34	0.60	1.63
760	0.09	0.13	0.24	0.30	0.52
762	0.07	0.10	0.22	0.65	0.86
Mean	0.09	0.13	0.27	0.48	0.95
Standard Dev.	0.02	0.03	0.05	0.17	0.39
Squared COV	0.05	0.04	0.04	0.12	0.17
Lognormal values:					
Variance	0.05	0.04	0.04	0.11	0.16
Mean	-2.41	-2.08	-1.31	-0.78	-0.13
Log Std. Dev.	0.23	0.21	0.19	0.34	0.39

The mean and standard deviation of these PGA values for different ground motions were then calculated for each limit state. The lognormal values of these measures were obtained using the lognormal transformation equations of Nowak and Collins, as presented in Equations 1 and 2 [30]. Notably, the standard deviation of the values generally increases with higher limit states. This observation is consistent with Figure 3, which showed greater dispersion in values at higher limit states.

Tables 5 to 8 present the specific PGA thresholds required to trigger each limit state across the seven ground motions for columns C1 through C4, along with their derived statistical parameters. These tables serve as the statistical foundation for the fragility assessment. By examining the mean PGA values across the tables, the direct impact of the longitudinal steel ratio on seismic capacity becomes evident. For instance, Column 1 (the stiffest column with a 6.55% steel ratio) requires a mean PGA of 1.85g to reach LS5 (5.0% drift). In contrast, Column 4 (the most flexible column with a 2.18% steel ratio) reaches the same limit state at a substantially lower mean PGA of 0.95g. This comparison quantifies the structural vulnerability associated with lower reinforcement ratios.

Furthermore, the statistical dispersion (captured by the standard deviation and coefficient of variation (COV)) provides critical insight into the structural response under different seismic excitations. At lower limit states (LS1 and LS2), the standard deviation remains relatively small across all columns, indicating that the columns respond predictably to different ground motions while still in the elastic or early yielding phases. However, as the columns progress toward extensive damage (LS4) and the 5.0% drift proxy (LS5), the standard deviation generally increases. This widening dispersion highlights that once substantial nonlinear degradation occurs, the structure's performance becomes highly sensitive to the specific characteristics of individual ground motions, such as frequency content and duration.

The lognormal mean and standard deviation values derived in these tables summarize this behavior and are subsequently substituted into Equation 3 to generate the continuous fragility curves, and the resulting exceedance probabilities at selected PGA levels are listed in Tables 9–12.

Table 9. Drift-threshold exceedance probabilities at selected PGA levels for C1

PGA (g)	Probability of Exceedance on Limit States				
	0.50%	**0.70%**	**1.50%**	**2.50%**	**5.00%**
0.10	19.51%	2.60%	0.00%	0.00%	0.00%
0.20	87.46%	60.37%	2.35%	0.01%	0.00%
0.30	98.99%	93.98%	21.37%	0.35%	0.00%
0.40	99.92%	99.32%	52.09%	3.20%	0.00%
0.50	99.99%	99.93%	76.08%	11.53%	0.00%
0.60	100.00%	99.99%	89.34%	25.31%	0.00%
0.70	100.00%	100.00%	95.53%	41.56%	0.00%
0.80	100.00%	100.00%	98.17%	57.06%	0.00%
0.90	100.00%	100.00%	99.26%	69.95%	0.00%
1.00	100.00%	100.00%	99.70%	79.72%	0.00%
1.50	100.00%	100.00%	100.00%	97.83%	3.22%
2.00	100.00%	100.00%	100.00%	99.79%	78.49%
2.50	100.00%	100.00%	100.00%	99.98%	99.77%
3.00	100.00%	100.00%	100.00%	100.00%	100.00%

The fragility curves for each column, developed from the seven ground motion records and illustrating the relationship between incremental PGA values and probabilities of exceedance for each limit state, are presented in Figure 4.

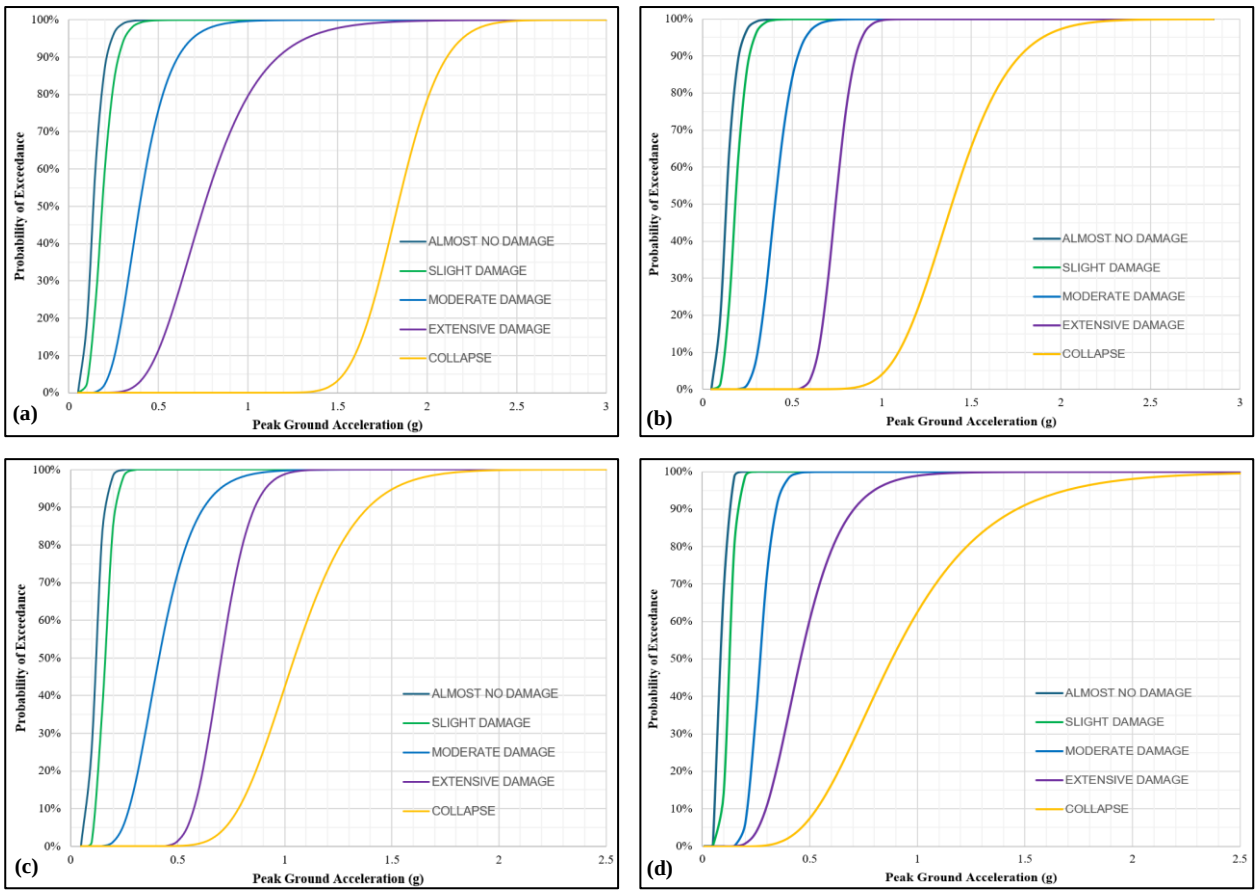


Figure 4. Fragility curves based on drift-ratio limit states for (a) C1, (b) C2, (c) C3, and (d) C4

As Figure 4 indicates, Column 1 (C1), characterized by the highest steel ratio, has the lowest probability of exceeding LS5. For example, at a PGA of 1.5g, C1 has only a 3.22% probability of exceeding LS5. Conversely, Column 4 (C4), which has the lowest stiffness, shows a much higher probability of 91.11% at the same PGA. This trend—that stiffer columns have a lower probability of exceedance at a given PGA—also holds for most other limit states. Furthermore, columns with higher steel ratios typically exhibit a lower or similar probability of exceedance at a given limit state than columns with lower steel ratios.

Table 10. Drift-threshold exceedance probabilities at selected PGA levels for C2

PGA (g)	Probability of Exceedance on Limit States				
	0.50%	**0.70%**	**1.50%**	**2.50%**	**5.00%**
0.10	19.94%	1.46%	0.00%	0.00%	0.00%
0.20	89.45%	62.63%	0.05%	0.00%	0.00%
0.30	99.34%	96.29%	8.09%	0.00%	0.00%
0.40	99.96%	99.76%	47.97%	0.00%	0.00%
0.50	100.00%	99.99%	84.01%	0.02%	0.00%
0.60	100.00%	100.00%	96.78%	2.58%	0.00%
0.70	100.00%	100.00%	99.49%	29.50%	0.01%
0.80	100.00%	100.00%	99.93%	75.18%	0.16%
0.90	100.00%	100.00%	99.99%	96.04%	1.02%
1.00	100.00%	100.00%	100.00%	99.67%	3.94%
1.50	100.00%	100.00%	100.00%	100.00%	65.57%
2.00	100.00%	100.00%	100.00%	100.00%	97.33%
2.50	100.00%	100.00%	100.00%	100.00%	99.91%
3.00	100.00%	100.00%	100.00%	100.00%	100.00%

Table 11. Drift-threshold exceedance probabilities at selected PGA levels for C3

PGA (g)	Probability of Exceedance on Limit States				
	0.50%	**0.70%**	**1.50%**	**2.50%**	**5.00%**
0.10	25.86%	1.14%	0.00%	0.00%	0.00%
0.20	98.35%	85.15%	1.16%	0.00%	0.00%
0.30	99.99%	99.86%	15.74%	0.00%	0.00%
0.40	100.00%	100.00%	45.73%	0.01%	0.00%
0.50	100.00%	100.00%	72.21%	1.41%	0.05%
0.60	100.00%	100.00%	87.66%	15.18%	0.64%
0.70	100.00%	100.00%	94.94%	48.27%	3.62%
0.80	100.00%	100.00%	98.01%	79.11%	11.53%
0.90	100.00%	100.00%	99.23%	94.10%	25.10%
1.00	100.00%	100.00%	99.70%	98.73%	42.10%
1.50	100.00%	100.00%	100.00%	100.00%	94.71%
2.00	100.00%	100.00%	100.00%	100.00%	99.82%
2.50	100.00%	100.00%	100.00%	100.00%	100.00%
3.00	100.00%	100.00%	100.00%	100.00%	100.00%

Table 12. Drift-threshold exceedance probabilities at selected PGA levels for C4

PGA (g)	Probability of Exceedance on Limit States				
	0.50%	**0.70%**	**1.50%**	**2.50%**	**5.00%**
0.05	0.51%	0.00%	0.00%	0.00%	0.00%
0.08	30.50%	1.60%	0.00%	0.00%	0.00%
0.10	68.01%	14.05%	0.00%	0.00%	0.00%
0.20	99.98%	98.71%	5.94%	0.73%	0.01%
0.30	100.00%	100.00%	71.87%	10.65%	0.31%
0.40	100.00%	100.00%	98.20%	34.66%	2.24%
0.60	100.00%	100.00%	100.00%	78.95%	16.41%
0.80	100.00%	100.00%	100.00%	95.11%	40.23%
1.00	100.00%	100.00%	100.00%	98.97%	62.51%
1.50	100.00%	100.00%	100.00%	99.98%	91.11%
2.00	100.00%	100.00%	100.00%	100.00%	98.11%
2.50	100.00%	100.00%	100.00%	100.00%	99.59%
3.00	100.00%	100.00%	100.00%	100.00%	99.91%
5.00	100.00%	100.00%	100.00%	100.00%	100.00%

To further investigate the effects of steel ratio, the fragility curves for each column corresponding to each limit state are developed and presented in Figure 5. As anticipated and consistent with previous discussions, columns with a higher steel ratio generally display a lower probability of exceedance for a particular limit state compared to those with a lower steel ratio (refer to Figure 5). However, a noteworthy observation emerges at Limit State 1 (LS1) and Limit State 2 (LS2): the difference in the probability of exceedance between C1 (ρ=6.55%) and C2 (ρ=4.19%) is very small. In contrast, the gap widens considerably for a smaller reduction in steel ratio. For example, the difference in steel ratio between C2 and C3 (ρ=2.79%) is smaller than that between C1 and C2, yet the difference in their probabilities of exceedance is considerably larger than that observed between C1 and C2.

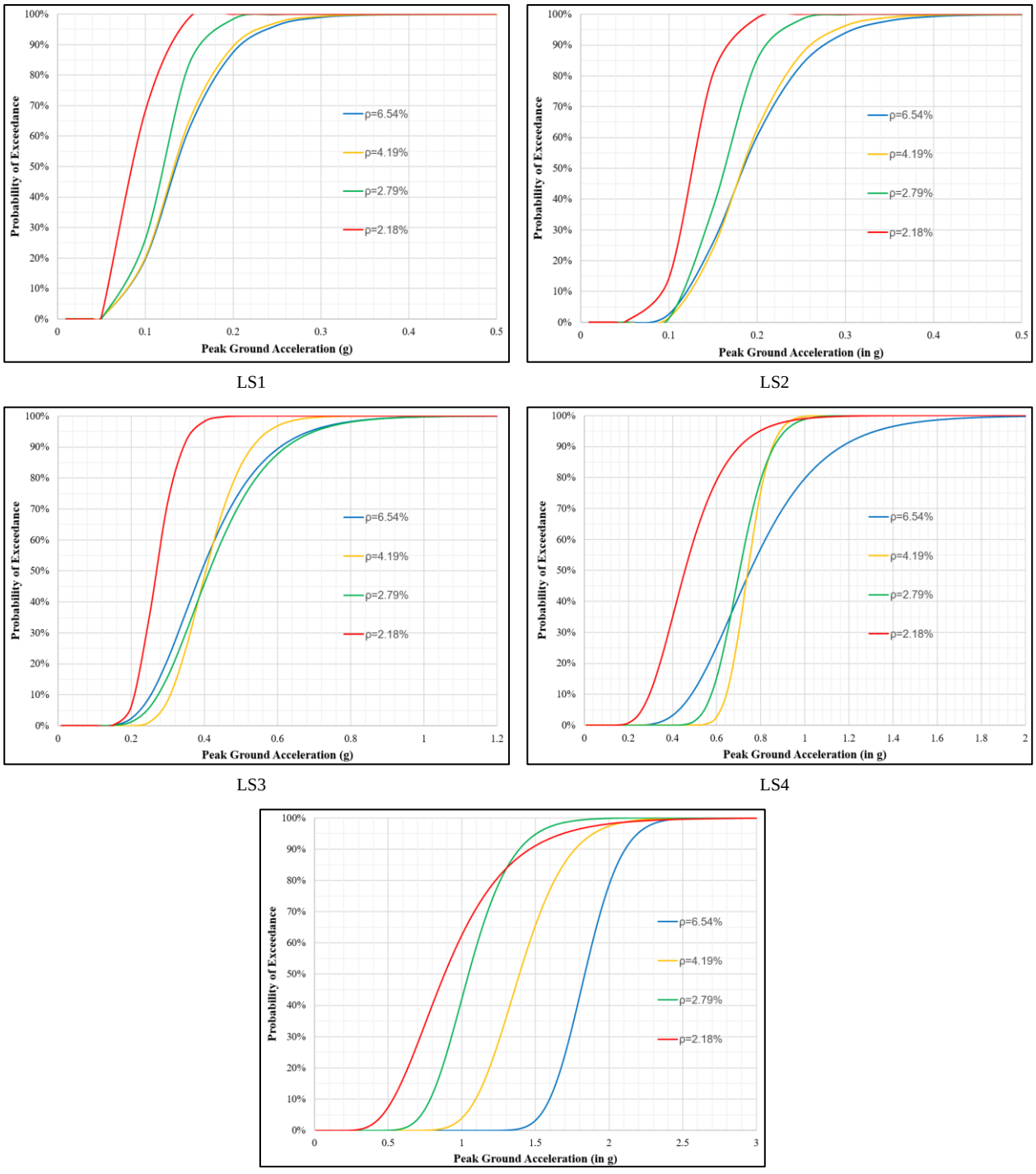


Figure 5. Fragility curves of columns at different limit states

Similarly, at Limit State 3 (LS3) and Limit State 4 (LS4), despite the small difference in steel ratio between C3 and C4, there is a large discrepancy in their probabilities of exceedance. Another interesting observation occurs at lower PGA values (0.2 to 0.4g): the stiffest column, C1, initially shows a higher probability of exceedance than C2 and C3. However, C2 and C3 eventually reach a 100% probability of exceedance before C1 does. At LS5 (5.0% drift), the differences in probabilities of exceedance broadly follow the change in steel ratio, so a smaller decrease in steel ratio generally corresponds to a smaller increase in the probability of exceedance, with the local exception noted below.

The ordering is not strictly monotonic at every intensity. The mean LS3 capacity of C3 was 0.44g, slightly greater than C1 (0.42g) and C2 (0.41g). At PGA = 0.40g, the LS3 exceedance probabilities were 52.09%, 47.97%, and 45.73% for C1, C2, and C3, respectively. At PGA = 1.50g, the LS5 probability for C3 (94.71%) also slightly exceeded C4 (91.11%). These reversals arise because both median capacity and logarithmic dispersion determine fragility, allowing curves to intersect. The results therefore do not support an invariant reinforcement-based ranking at every PGA.

The general tendency for reinforcement configuration to affect cyclic response is consistent with earlier column research [9] and recent calibrated experimental–numerical studies [14, 18]. Contemporary fragility analyses likewise show that configuration, deterioration, and record-to-record variability can shift the location and dispersion of RC pier fragility curves [16, 17]. Direct numerical agreement should not be expected because those studies used different geometries, axial loads, damage measures, failure mechanisms, and ground-motion ensembles. Zhang et al. [15] further showed that drift alone may not fully reproduce observed physical damage, supporting the cautious interpretation adopted here.

4. Conclusion

This simulation-based study quantified the influence of longitudinal-reinforcement ratio on the drift fragility of four otherwise comparable 300 × 300 mm, 4.0 m reinforced-concrete cantilever-column models. Reinforcement ratios of 6.55%, 4.19%, 2.79%, and 2.18% were assigned to C1–C4, respectively. Nonlinear time-history analyses were conducted in SeismoStruct using seven records from the 1989 Loma Prieta earthquake, with peak ground acceleration (PGA) as the intensity measure and maximum drift ratio as the engineering demand parameter. PGA values corresponding to five prescribed drift thresholds were represented by lognormal fragility functions. At the 5.00% threshold, the mean PGA decreased systematically from 1.85g for C1 to 1.42g, 1.07g, and 0.95g for C2, C3, and C4. At 1.0g, the calculated probabilities of exceeding this threshold were 0.00%, 3.94%, 42.10%, and 62.51%, respectively. The C1–C4 difference in mean PGA increased from only 0.05g at the 0.50% threshold to 0.90g at the 5.00% threshold. This indicates that the influence of reinforcement ratio became clearer at severe drift demands. However, this influence was not uniform across all limit states: C1 and C2 had identical rounded means at 0.50% and 0.70% drift, and C3 slightly exceeded C1 and C2 at 1.50% drift. Fragility-curve shifts therefore cannot be assumed proportional to changes in steel ratio, particularly at low and intermediate response levels.

The findings describe numerical drift-threshold exceedance, not experimentally observed damage or physical collapse. In particular, LS5 is an assumed 5.00% drift proxy and does not demonstrate dynamic instability, loss of axial-load capacity, shear failure, reinforcement buckling, or bond-slip failure. Generalization is also constrained by the use of seven records from one earthquake and PGA as the sole intensity measure. Future research should validate stiffness, strength, and cyclic deterioration against laboratory tests or an established benchmark; include records from multiple events and site classes; and compare PGA with spectral acceleration at each model's fundamental period. Explicit representation of shear, bar buckling, bond slip, confinement, and different axial-load ratios would further clarify the observed trends. Within these limits, the study provides a controlled quantitative basis for assessing how longitudinal reinforcement can modify simulated RC-column drift fragility.

5. Declarations

5.1. Author Contributions

Conceptualization, J.R.P.G.L.; methodology, L.C.M.D.J. and F.F.M.; software, L.C.M.D.J.; simulation, J.R.P.G.L.; validation, A.A., S.M., and K.M.; formal analysis, J.R.P.G.L.; investigation, F.F.M. and K.M.; resources, A.A.; data curation, S.M.; writing—original draft preparation, F.F.M. and K.M.; writing—review and editing, L.C.M.D.J., A.A., and S.M.; visualization, K.M.; supervision, F.F.M.; project administration, A.A.; funding acquisition, S.M. All authors have read and agreed to the published version of the manuscript.

5.2. Data Availability Statement

The data presented in this study are available on request from the corresponding author.

5.3. Funding

This research received no external funding. The article processing fee was funded by Asia Pacific College.

5.4. Conflicts of Interest

The authors declare no conflict of interest.

6. References

[1] Vamvatsikos, D., & Cornell, C. A. (2002). Incremental dynamic analysis. Earthquake Engineering and Structural Dynamics, 31(3), 491–514. doi:10.1002/eqe.141.

[2] Barbat, A. H., Vargas, Y. F., Pujades, L. G., & Hurtado, J. E. (2016). Probabilistic seismic risk assessment of structures based on stiffness degradation. Revista Internacional de Metodos Numericos Para Calculo y Diseno En Ingenieria, 32(1), 39–47. doi:10.1016/j.rimni.2014.11.001. (In Spanish).

[3] Vargas, Y. F., Pujades, L. G., Barbat, A. H., & Hurtado, J. E. (2015). Probabilistic Seismic Damage Assessment of RC Buildings Based on Nonlinear Dynamic Analysis. The Open Civil Engineering Journal, 9(1), 344–350. doi:10.2174/1874149501509010344.

[4] Wang, Q. W., Shi, Q. X., & Men, J. J. (2011). Seismic performance evaluation of SRC frames based on incremental dynamic analysis. Advanced Materials Research, 163–167, 4331–4335. doi:10.4028/www.scientific.net/AMR.163-167.4331.

[5] Mokhtari, M., & Naderpour, H. (2022). Seismic vulnerability assessment of reinforced concrete buildings having nonlinear fluid viscous dampers. Bulletin of Earthquake Engineering, 20(13), 7675–7704. doi:10.1007/s10518-022-01508-7.

[6] Dadkhah, M., Kamgar, R., & Heidarzadeh, H. (2022). Reducing the Cost of Calculations for Incremental Dynamic Analysis of Building Structures Using the Discrete Wavelet Transform. Journal of Earthquake Engineering, 26(7), 3317–3342. doi:10.1080/13632469.2020.1798830.

[7] Li, N., Zhai, C. H., & Xie, L. L. (2011). Simplified incremental dynamic analysis method for uniaxial plan-asymmetric structures. Gongcheng Lixue/Engineering Mechanics, 28(5), 8–12.

[8] Azarbakht, A., & Dolšek, M. (2011). Progressive Incremental Dynamic Analysis for First-Mode Dominated Structures. Journal of Structural Engineering, 137(3), 445–455. doi:10.1061/(asce)st.1943-541x.0000282.

[9] Trejo, D., Link, T. B., & Barbosa, A. R. (2016). Effect of reinforcement grade and ratio on seismic performance of reinforced concrete columns. ACI Structural Journal, 113(5), 907–916. doi:10.14359/51689015.

[10] Xu, S., Wu, C., Liu, Z., & Li, J. (2018). Numerical study of ultra-high-performance steel fibre–reinforced concrete columns under monotonic push loading. Advances in Structural Engineering, 21(8), 1234–1248. doi:10.1177/1369433217747710.

[11] Sun, W., & Li, S. (2022). Mechanical Property Analysis and Calculation Method Modification of Steel-Reinforced High-Strength Concrete Columns. Materials, 15(19), 6863. doi:10.3390/ma15196863.

[12] Xiamuxi, A., Liu, C., & Jierula, A. (2023). Study of the longitudinal reinforcement in reinforced concrete-filled steel tube short column subjected to axial loading. Steel and Composite Structures, 47(6), 709–728. doi:10.12989/scs.2023.47.6.709.

[13] Aldabagh, S., Hossain, F., & Alam, M. S. (2024). Refined deformation limit states for circular reinforced concrete bridge columns. Earthquake Engineering and Structural Dynamics, 53(1), 348–365. doi:10.1002/eqe.4023.

[14] Di Domenico, M., Barbagallo, F., Terrenzi, M., Cantagallo, C., Ricci, P., Camata, G., Marino, E. M., Spacone, E., & Verderame, G. M. (2025). Fiber modelling approach for seismic analysis of flexure-controlled RC columns with ribbed bars calibrated on unidirectional experimental tests. Bulletin of Earthquake Engineering, 23(10), 3953–3984. doi:10.1007/s10518-025-02211-z.

[15] Zhang, H., Mao, C., & Zhou, W. (2025). Damage evaluation of experimental reinforced concrete cantilever columns under bidimensional loading using Diem. Bulletin of Earthquake Engineering, 23(11), 4429–4462. doi:10.1007/s10518-025-02194-x.

[16] Khan, M. S., & Rizwan, M. (2025). Fragility and vulnerability assessment of code-conforming and non-conforming RC Bridge piers retrofitted with ECC jackets. Journal of Building Pathology and Rehabilitation, 10(2), 107. doi:10.1007/s41024-025-00616-6.

[17] Perrone, G., Cardone, D., & Possidente, V. (2025). Collapse fragility curves of RC piers with corroded rebars. Bulletin of Earthquake Engineering, 23(10), 4255–4282. doi:10.1007/s10518-025-02202-0.

[18] John, S. K., Cascardi, A., Verre, S., & Nadir, Y. (2025). RC-columns subjected to lateral cyclic force with different FRCM-strengthening schemes: experimental and numerical investigation. Bulletin of Earthquake Engineering, 23(4), 1561–1590. doi:10.1007/s10518-025-02100-5.

[19] Lee, B. G., An, J. H., Kim, K., Jung, J. S., & Lee, K. S. (2026). Experimental and non-linear FEA-based seismic evaluation of corroded flexural and shear R/C columns. Bulletin of Earthquake Engineering, 24(8), 6281–6317. doi:10.1007/s10518-026-02465-1.

[20] Shang, J., Pan, Z., & Zeng, B. (2025). Seismic vulnerability analysis of local prestressed concrete frame with varying partial prestressing ratio based on incremental dynamic analysis. Journal of Building Engineering, 111, 113398. doi:10.1016/j.jobe.2025.113398.

[21] Vielma, J. C., & Cando, M. A. (2017). Evaluation of the behavior factor in the Ecuadorian Building Code for steel moment-resisting frame structures. Revista Internacional de Metodos Numericos Para Calculo y Diseno En Ingenieria, 33(3–4), 271–279. doi:10.1016/j.rimni.2016.09.001.

[22] Asgarian, B., & Jalaeefar, A. (2011). Incremental dynamic analysis of steel braced frames designed based on the first, second and third editions of the Iranian seismic code (standard no. 2800). Structural Design of Tall and Special Buildings, 20(2), 190–207. doi:10.1002/tal.528.

[23] Mander, J. B., Priestley, M. J. N., & Park, R. (1988). Theoretical Stress-Strain Model for Confined Concrete. Journal of Structural Engineering, 114(8), 1804–1826. doi:10.1061/(asce)0733-9445(1988)114:8(1804).

[24] Menegotto, M., & Pinto, P. E. (1973). Method of analysis for cyclically loaded RC plane frames including changes in geometry and non-elastic behavior of elements under combined normal force and bending. Proc. of IABSE Symposium on Resistance and Ultimate Deformability of Structures Acted on by Well Defined Repeated Loads, 13-14 September, 1973, Lisbon, Portugal.

[25] Han, Q., Zhou, Y. L., & Du, X. L. (2015). Seismic performance of reinforced concrete rectangular hollow bridge columns. Gongcheng Lixue/Engineering Mechanics, 32(3), 28–40. doi:10.6052/j.issn.1000-4750.2013.11.1020.

[26] Sezen, H., & Moehle, J. P. (2004). Shear Strength Model for Lightly Reinforced Concrete Columns. Journal of Structural Engineering, 130(11), 1692–1703. doi:10.1061/(asce)0733-9445(2004)130:11(1692).

[27] Kim, S. H., & Shinozuka, M. (2004). Development of fragility curves of bridges retrofitted by column jacketing. Probabilistic Engineering Mechanics, 19(1), 105–112. doi:10.1016/j.probengmech.2003.11.009.

[28] Dutta, A., & Mander, J. B. (1999). Seismic fragility analysis of highway bridges. Proceedings of the INCEDE-MCEER Center-to-Center Project Workshop on Earthquake Engineering Frontiers in Transportation Systems, Tokyo, Japan.

[29] PEER. (2025). PEER Ground Motion Database. Pacific Earthquake Engineering Research Center, PEER NGA WEST 2, University of California, Berkeley, United States. Available online: https://ngawest2.berkeley.edu/ (accessed on September 2026).

[30] Nowak, A. S., & Collins, K. R. (2012). Reliability of Structures. CRC Press, London, United Kingdom. doi:10.1201/b12913.

[31] U.S. Geological Survey. (2024). M 6.9 October 17, 1989 Loma Prieta Earthquake. U.S. Geological Survey, Reston, United States. Available online: https://www.usgs.gov/programs/earthquake-hazards/science/m-69-october-17-1989-loma-prieta-earthquake (accessed on September 2026).